SIMULATION OF PLASMA DECHIRPER AND LENS FOR LASER WAKEFIELD ACCELERATION*

T. L. Steyn†, C. Ballage, B. Cros, P. Désesquelles, O. Khomyshyn, M. Masckala,
F. Massimo, I. Moulanier, O. Vasilovici, LPGP, CNRS, Université Paris Saclay, Orsay, France
S. Dobosz Dufrénoy, A. Panchal, LIDYL, CEA, Université Paris Saclay, Gif-sur-Yvette, France
Y.-Yu Chang, A. Irman, M. Laberge, S. Schöbel, F. M. Herrmann[1], M. Samir[1], U. Schramm[1], P. Ufer[1]
Helmholtz-Zentrum Dresden-Rossendorf, Dresden, Germany
[1] also at Technische Universität Dresden, Dresden, Germany

Abstract

Laser wakefield accelerators can produce compact, high-gradient electron sources, but typically generate chirped beams with significant energy spread and divergence. We present a simulation study of a tailored plasma density profile that performs post-acceleration phase-space manipulation within a single gas-cell target: a plasma down-ramp providing transverse lensing and a long, low-density plasma tail acting as a beam-driven dechirper and lens. Using OpenFOAM fluid simulations to generate the density profile and Particle-in-Cell simulations to resolve the wakefields, we analyze the longitudinal and transverse fields responsible for chirp generation, dechirping, and collimation.

INTRODUCTION

Laser wakefield acceleration (LWFA) produces relativistic electron beams over mm-scale distances using the large longitudinal electric fields sustained by plasma waves [1–3]. In the laser-driven blowout-regime configuration considered here, the accelerated bunch spans a finite fraction of the accelerating phase, so the longitudinal field varies along the bunch length; different longitudinal slices therefore accumulate different energy gains, imprinting a head–tail energy–position correlation (chirp). In particular, situations where the rear of the bunch experiences a higher accelerating field lead to a positive chirp. Although optimal beam loading [4, 5] can mitigate these effects, it imposes strict requirements on the longitudinal charge distribution [6, 7]. In addition, the beam must be extracted and transported with minimal transverse momentum spread.

Here we give a fuller description of how the wakefields in the accelerating phase lead to chirped beams and how the post-acceleration fields remove this imposed chirp, as first described in [8, 9] and elsewhere in this conference as [10]. We model a compact plasma structure including: (i) a plasma density down-ramp that behaves as a lens, reducing transverse momentum spread via the transverse wake focusing forces generated by the wakefield driven by the laser [11, 12]; and (ii) a long, low-density plasma tail (LPT) where the electron bunch drives its own wakefield, providing simultaneous focusing and dechirping.

SIMULATION MODELS

The longitudinal plasma density distribution is obtained from computational fluid dynamics simulations of a two-compartment gas cell and a downstream channel using OpenFOAM [13, 14]. The simulated neutral density distribution (hydrogen and nitrogen) is converted to an electron density profile for the PIC input. The density profile of a simulation where the pressure is equal between the two compartments is shown in Fig. 1. The mesh lines are coloured based on the local concentration of nitrogen in the gas. Black lines indicates parts where the nitrogen concentration is high (close to 15%), which is the concentration of gas in the reservoir providing nitrogen to the first compartment (C1) in this simulation. White lines indicate the absence of nitrogen. Thus having the pressures equal in both compartments leads to proper confinement of the nitrogen in the first compartment. The gradient of the nitrogen concentration between the two compartments leads to an electron density down-ramp which is where the ionisation injection occurs.

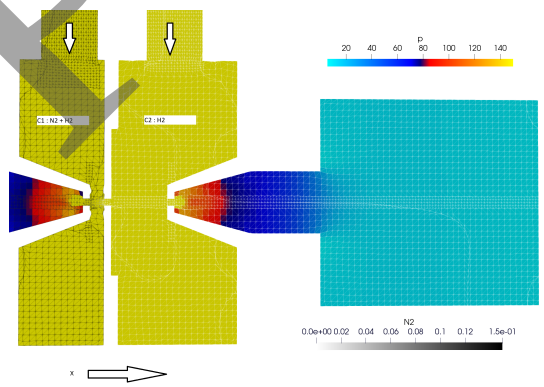

Figure 1: OpenFOAM simulation of the gas-cell exit and low-density tail. The horizontal arrow denotes the laser propagation direction. The first compartment (C1) is filled with a mixture of hydrogen and nitrogen. The fraction nitrogen is indicated by the colour of the mesh lines. The second compartment (C2) is filled with pure hydrogen. The pressure here is shown as the color map of the background in units of Pa.

The maximum value the pressure scale of the profile is intentionally saturated to show the low density structure that forms in the outlet of the gas cell (C2). This structure is particularly important as it forms the plasma lens and

* arXiv:2604.26486
† theunis-lodewyk.steyn@universite-paris-saclay.fr

dechirper for the accelerated bunch. This structure is formed by the geometric constriction around the primary outlet of the gas cell, which leads to a low-density tail extending over several millimeters. The gas density profile obtained from the OpenFOAM simulations is converted to electron and ion density profiles as input for the PIC simulations.

PIC simulations of the injection, acceleration, and post-acceleration dynamics were performed with Smilei [15] using a quasi-cylindrical geometry with azimuthal Fourier decomposition [16]. The laser is initialized as a focused flattened-Gaussian beam [17] with 30 fs (FWHM) pulse duration and peak normalized vector potential $a_0 \approx 2.3$ at focus, where $a_0 = eE_0/(m_e c\omega_0)$, E_0 is the peak laser electric-field amplitude, and $\omega_0 = 2\pi c/\lambda_0$ is the laser angular frequency. In the following, x denotes the longitudinal coordinate (laser propagation direction). We track (i) the evolution of the laser peak amplitude a_0, (ii) the transverse momentum spread, and (iii) the evolution of the longitudinal phase space and the energy chirp.

CHIRP, LENSING, AND DECHIRPING

Figure 2 summarizes the simulated evolution of the laser and electron beam along the tailored density profile. During the injection/acceleration stages ($x < 3.5$ mm), the laser-driven wake provides strong longitudinal accelerating gradients while betatron oscillations are visible in the transverse momentum spread in the middle panel. In the second down-ramp ($3.5 < x < 6$ mm) at the exit of the gas cell (C2) the wake focusing fields act as a plasma lens and reduce the transverse momentum spread. The bottom graph shows that the energy spread increases during acceleration, but then decreases in the LPT, while simultaneously the charge within the FWHM increases. Detailed analysis shows that the energy spread is high at the end of the acceleration stage because of the strong energy–position correlation (chirp) imprinted on the bunch by the non-uniform longitudinal field structure. The subsequent LPT provides a beam-driven wakefield that compensates this chirp, leading to a reduction in energy spread while also providing additional focusing of the bunch.

To connect these beam observables to the underlying wake structure, we analyze snapshots of the longitudinal accelerating field and the transverse wakefield component responsible for focusing at characteristic positions along the profile. The chirp is generated while the bunch overlaps the accelerating phase of the wake: because the longitudinal field varies across the bunch length, different longitudinal slices accumulate different energy gains. Figure 3 shows the field structure at $x \approx 4.3$ mm close to peak laser amplitude.

Fig. 3 (a) shows that the bunch extends over 10 μm, and that the longitudinal field structure is non-uniform across the bunch length, with stronger gradients at the back of the cavity. This leads to a significant chirp imprinted on the bunch during acceleration. The transverse wakefield component is shown in Fig. 3 (b): the bunch experiences intense focusing forces throughout its length leading to the betatron

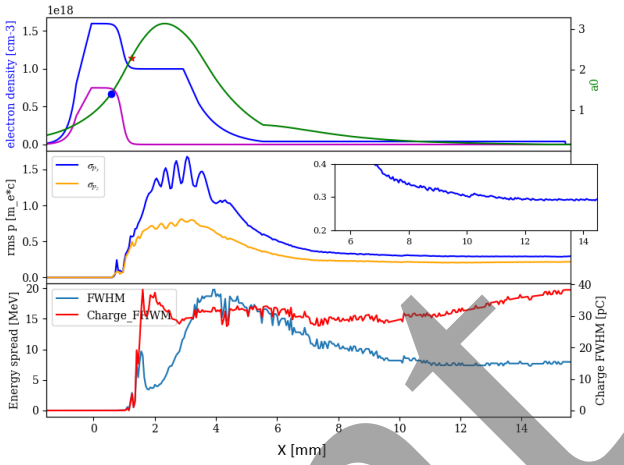

Figure 2: Simulation summary along the tailored density profile. Top: evolution of laser peak amplitude a_0(green line), Electron density (blue) and nitrogen density(purple). Middle: transverse momentum spread of the accelerated bunch, blue in the y-direction(polarisation of the laser), orange in the z-direction. Bottom: evolution of the energy spread (FWHM) in blue and the charge contained within the FWHM of the energy spectrum in red.

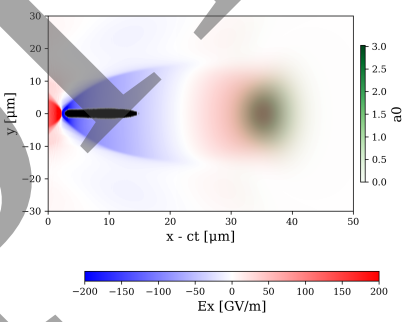

(a)

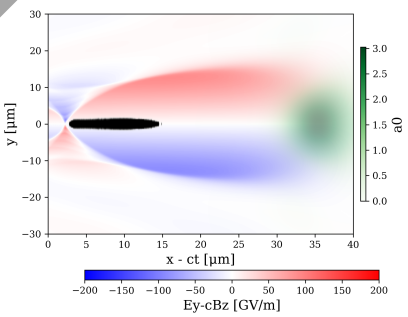

(b)

Figure 3: Field snapshots in the laser-driven stage at $x \approx 4.3$ mm. Electron beam in black. The green color map is the laser intensity. (a) Longitudinal field E_x with the electron bunch. (b) Transverse wakefield component responsible for focusing/defocusing (and the laser intensity).

oscillations and the associated transverse momentum spread oscillations observed in the middle panel of Fig. 2.

After the down-ramp $x > 6$ mm, the laser amplitude is strongly depleted. In the LPT, the bunch density becomes

comparable to (or exceeds) the plasma density, and the wakefield becomes predominantly beam-driven. In this regime, the head of the bunch excites a wakefield such that the tail experiences a longitudinal field of opposite sign relative to the initial chirp, reducing the energy–position correlation (dechirping). The same beam-driven wake provides transverse focusing, contributing to additional collimation (Fig. 4). This explains the reduction in energy spread and the increase in the charge contained within the FWHM of the energy spectrum observed in the bottom panel of Fig. 2 in the LPT. In the transverse direction, the field generated by the beam driven wakefield in the LPT provides additional focusing of the bunch, specifically to those particles in the rear of the bunch. The rear of the beam thus experiences relaxation over a longer distance, which leads to a lower transverse momentum spread for the beam as a whole. This is observed in the middle panel of Fig. 2 where the transverse momentum spread decreases in the LPT.

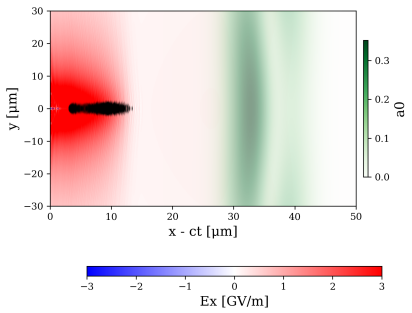

(a)

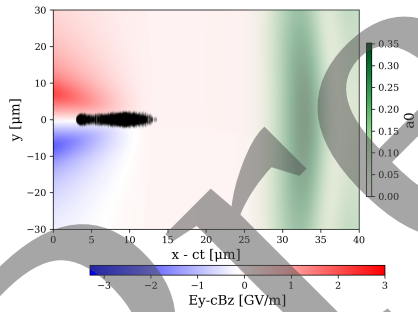

(b)

Figure 4: Field snapshots in the LPT at $x \approx 10$ mm. (a) Longitudinal field structure associated with the beam-driven wakefield, providing energy chirp compensation. (b) Transverse wakefield component, providing additional focusing of the bunch in the LPT.

The evolution of the longitudinal phase space at 3 positions along the density profile is shown in Fig. 5. At the end of the acceleration stage at x = 3.5 mm, the bunch has a significant chirp due to the non-uniform longitudinal field structure shown in Fig. 3. After the down-ramp at x = 6 mm, this correlation mostly remains, however at the end of the low-density tail at x = 15 mm, the beam driven wakefield (dechirper) has reduced the chirp, and energy spread, significantly. This simulation is compared with an experimental spectra measured in experiment using the laser and density profile modeled here, as shown in [8]. The experimental result is shown here as a black dashed line.

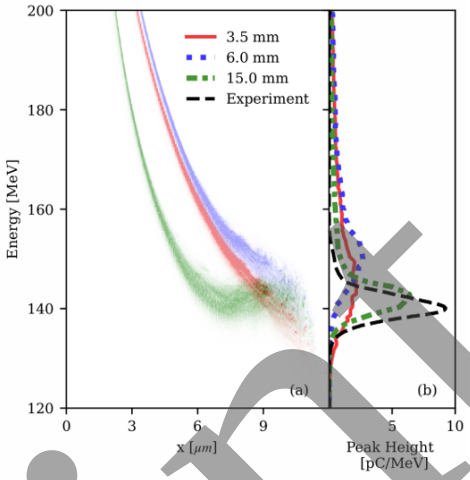

Figure 5: Evolution of the longitudinal phase space (chirp) at three positions. The beam-driven wakefield in the low-density tail reduces the initial energy–position correlation acquired during acceleration.

The net effect on the bunch chirp is summarized in Fig. 5: the bunch exits the acceleration stage with a significant chirp, which is progressively reduced along the low-density tail. The same tail contributes transverse focusing, so the device acts as a combined plasma lens and dechirper. We have shown here how the field structure in the accelerating stage leads to chirp generation, and how the subsequent beam-driven wakefield in the low-density tail provides simultaneous dechirping and focusing, leading to a reduction in energy spread and transverse momentum spread.

CONCLUSION

Using OpenFOAM-derived density profiles and Smilei PIC simulations, we have analyzed a tailored plasma structure that provides post-acceleration transverse lensing and longitudinal dechirping for LWFA electron beams. The field snapshots show how strong longitudinal-field gradients imprint a chirp during the laser-driven stage, while the subsequent low-density tail is dominated by beam-driven wakefields that compensate the chirp and further focus the bunch.

ACKNOWLEDGEMENTS

This work was granted access to the HPC resources of TGCC and CINES under the allocations 2023-A0150510062, 2024-A0170510062 (Virtual Laplace) and 2025-A0190510062 made by GENCI. The authors acknowledge M. Bisson for the design and management of the MAITRO HPC cluster at LPGP.

REFERENCES

[1] E. Esarey, C. B. Schroeder, and W. P. Leemans, "Physics of laser-driven plasma-based electron accelerators", *Rev. Mod. Phys.*, vol. 81, no. 3, pp. 1229–1285, 2009. doi:10.1103/RevModPhys.81.1229

[2] S. M. Hooker, "Developments in laser-driven plasma accelerators", *Nat. Phot.*, vol. 7, no. 10, pp. 775–782, 2013. doi:10.1038/nphoton.2013.234

[3] M. C. Downer, R. Zgadzaj, A. Debus, U. Schramm, and M. C. Kaluza, "Diagnostics for plasma-based electron accelerators", *Rev. Mod. Phys.*, vol. 90, no. 3, 2018. doi:10.1103/RevModPhys.90.035002

[4] C. A. Lindström *et al.*, "Energy-spread preservation and high efficiency in a plasma-wakefield accelerator", *Phys. Rev. Lett.*, vol. 126, no. 1, p. 014801, 2021. doi:10.1103/PhysRevLett.126.014801

[5] M. Kirchen *et al.*, "Optimal beam loading in a laser-plasma accelerator", *Phys. Rev. Lett.*, vol. 126, p. 174801, 2021. doi:10.1103/PhysRevLett.126.174801

[6] M. Tzoufras *et al.*, "Beam loading in the nonlinear regime of plasma-based acceleration", *Phys. Rev. Lett.*, vol. 101, no. 14, p. 145002, 2008. doi:10.1103/PhysRevLett.101.145002

[7] M. Tzoufras *et al.*, "Beam loading by electrons in nonlinear plasma wakes", *Phys. Plasma*, vol. 16, no. 5, p. 056705, 2009. doi:10.1063/1.3118628

[8] T. L. Steyn, A. Panchal, O. Vasilovici, *et al.*, Plasma dechirper and lens for electron beams from laser wakefield acceleration in a tailored density profile, 2026, doi:10.48550/arXiv.2604.26486

[9] T. L. Steyn, A. Panchal, O. Vasilovici, *et al.*, Observation of laser plasma accelerated electrons with transverse momentum spread below the thermal level, 2025, doi:10.48550/arXiv.2506.18047

[10] B. CROS *et al.*, "High quality electron beams with tunable energy produced by laser-plasma acceleration", presented at IPAC'26, Deauville, France, May 2026, paper TUI3T01, this conference,

[11] S. Kuschel *et al.*, "Demonstration of passive plasma lensing of a laser wakefield accelerated electron bunch", *Phys. Rev. Accel. Beams*, vol. 19, p. 071301, Jul. 2016. doi:10.1103/PhysRevAccelBeams.19.071301

[12] J. Björklund Svensson *et al.*, "Low-divergence femtosecond X-ray pulses from a passive plasma lens", *Nat. Phys.*, vol. 17, no. 5, pp. 639–645, May 2021. doi:10.1038/s41567-020-01158-z

[13] H. G. Weller, G. Tabor, H. Jasak, and C. Fureby, "A tensorial approach to computational continuum mechanics using object-oriented techniques", *Computers in Physics*, vol. 12, no. 6, pp. 620–631, 1998. doi:10.1063/1.168744

[14] OpenFOAM: the open source CFD toolbox, https://www.openfoam.com/

[15] J. Derouillat, A. Beck, F. Périllot, F. Vicini, *et al.*, "Smilei: a collaborative, open-source, multi-purpose particle-in-cell code for plasma simulation", *Comput. Phys. Commun.*, vol. 222, pp. 351–373, 2018. doi:10.1016/j.cpc.2017.09.024

[16] A. F. Lifschitz *et al.*, "Particle-in-cell modelling of laser–plasma interaction using a cylindrical geometry", *Comput. Phys. Commun.*, vol. 180, no. 12, pp. 2428–2445, 2009. doi:10.1016/j.jcp.2008.11.017

[17] M. Santarsiero, R. Borghi, *et al.*, "Approximate analytical description of flattened gaussian beams", *J. Opt. Soc. Am. A*, vol. 14, no. 10, pp. 2442–2453, 1997.